Journal of Biomolecular NMR (2018) 72:1–10
https://doi.org/10.1007/s10858-018-0201-6

ARTICLE

Structural investigation of glycan recognition by the ERAD quality control lectin Yos9

Andreas Kniss[1] · Sina Kazemi[1] · Frank Löhr[1] · Maren Berger[2] · Vladimir V. Rogov[1] · Peter Güntert[1,3,4] · Thomas Sommer[2,5] · Ernst Jarosch[2] · Volker Dötsch[1]

Received: 24 May 2018 / Accepted: 30 July 2018 / Published online: 31 July 2018

Abstract

Yos9 is an essential component of the endoplasmic reticulum associated protein degradation (ERAD) system that is responsible for removing terminally misfolded proteins from the ER lumen and mediating proteasomal degradation in the cytosol. Glycoproteins that fail to attain their native conformation in the ER expose a distinct oligosaccharide structure, a terminal α1,6-linked mannose residue, that is specifically recognized by the mannose 6-phoshate receptor homology (MRH) domain of Yos9. We have determined the structure of the MRH domain of Yos9 in its free form and complexed with 3α, 6α-mannopentaose. We show that binding is achieved by loops between β-strands performing an inward movement and that this movement also affects the entire β-barrel leading to a twist. These rearrangements may facilitate the processing of client proteins by downstream acting factors. In contrast, other oligosaccharides such as 2α-mannobiose bind weakly with only locally occurring chemical shift changes underscoring the specificity of this substrate selection process within ERAD.

Keywords Endoplasmatic reticulum associated protein degradation · Yos9 · Glycan binding · Conformational change

Introduction

Chaperones are essential components of the cellular protein production machinery that ensure that proteins adopt well folded structures to avoid aggregation. However, despite many, also organelle specific chaperone systems, folding can terminally fail, requiring the destruction of the misfolded protein either by the proteasomal pathway or by autophagy. Quality control of newly synthesized membrane proteins as well as soluble proteins of the secretory pathway is ensured in the lumen of the endoplasmic reticulum by a process called endoplasmic reticulum associated protein degradation (ERAD) (Werner et al. 1996). Cotranslational modification of polypeptides with preassembled asparagine-linked oligosaccharide structures serves as a marker and timer for the folding process in order to distinguish folding intermediates from terminally misfolded proteins (Aebi 2013; Braakman and Bulleid 2011). Chaperone-mediated folding is accompanied by a successive trimming of this oligosaccharide by glucosidases and mannosidases to yield a $Man_8GlcNAc_2$ moiety. This structure is found on the majority of glycoproteins by the time they leave the ER and thus after passing the quality control system. Further trimming of this oligosaccharide structure by Htm1/Mnl1 in yeast creates a terminal α1,6 mannose on its C-branch (Clerc et al. 2009; Jakob et al. 2001) within a $Man_7GlcNAc_2$ construct which can be selectively bound by Yos9 as part of the substrate selection process in ERAD. The exposed α1,6 mannose constitutes a selective recognition signal for binding to Yos9 (Hosokawa et al. 2009; Quan et al. 2008; Szathmary et al. 2005). The mannosidase Htm1 is tightly associated with the protein-oxidoreductase Pdi1 and preferentially processes glycoproteins that display a prolonged interaction with Pdi1 due to their abnormal conformation (Gauss et al. 2011; Pfeiffer et al.

✉ Volker Dötsch
vdoetsch@em.uni-frankfurt.de

1 Institute of Biophysical Chemistry and Center for Biomolecular Magnetic Resonance, Goethe University, Max-von-Laue Str. 9, 60438 Frankfurt am Main, Germany

2 Max-Delbrück Center for Molecular Medicine, Robert-Rössle-Str. 10, 13125 Berlin-Buch, Germany

3 Laboratory of Physical Chemistry, ETH Zurich, Vladimir-Prelog-Weg 2, 8093 Zurich, Switzerland

4 Graduate School of Science, Tokyo Metropolitan University, 1-1 Minami-ohsawa, Hachioji, Tokyo 192-0397, Japan

5 Institute for Biology, Humboldt Universität zu Berlin, Invalidenstrasse 43, 10115 Berlin, Germany

2016). The substrate selection process is further refined by Hrd3, which is associated with Yos9, and thought to additionally interact with surface-exposed unstructured regions on client proteins. The misfolded protein is subsequently handed over to transmembrane components of the HMG-CoA reductase degradation complex (HRD). The HRD complex translocates the protein to the cytosol and catalyzes K48-linked polyubiquitin chain formation on client proteins to target them for cytosolic degradation by the proteasome (von Delbruck et al. 2016).

In yeast, the crucial task of recognizing the trimmed oligosaccharide is carried out by the mannose-6-phosphate receptor homology (MRH) domain of Yos9. MRH domains are a common feature in many proteins involved in the secretory pathway. Examples are the β subunit of ER glucosidase II or the γ subunit of Golgi GlcNAc-phosphotransferase (D'Alessio and Dahms 2015).

Here, we solved the structure of the Yos9 MRH domain by solution NMR in two distinct conformational states: in a free form and bound to the minimal mannosyl oligosaccharide structure that is also exposed on ERAD substrates. We also performed interaction studies with other oligosaccharides that display no similarity to degradation signals for ERAD. Our data suggest that the binding of a cognate glycan induces conformational changes in Yos9, which may promote the processing of client molecules by downstream-acting components of the HRD-ligase complex.

Materials and methods

Protein purification

Yos9 MRH constructs were cloned into a modified pet28a vector and expressed as His6-GB1-tagged fusion proteins in T7 Express Competent E. coli cells (NEB) in M9 medium. Cells were grown to an optical density (600 nm) of 1.0 and induced with isopropyl-β−D−1−thiogalactopyranoside (IPTG) (0.5 mM) at 24 °C for 20 h. Yos9 was purified from inclusion bodies after solubilization in buffer containing 50 mM Tris (pH 7.8), 250 mM NaCl, 1% glycerol, 20 mM imidazole and 6 M urea and subsequently purified via Ni–NTA chromatography. Purified His6-GB1-Yos9(MRH) fusion proteins were diluted to 0.5 mg/mL using buffer containing 100 mM Tris (pH 8.5), 150 mM NaCl and 7 M urea and dialyzed overnight against buffer containing 100 mM Tris (pH 8.5), 150 mM NaCl, 1 mM $CaCl_2$, 0.5 M arginine, 5 mM GSH, 0.5 mM GSSG. A high pH favors disulfide bond formation since the reaction involves one sulfhydryl group acting as a nucleophile. In addition, a redox system (GSH:GSSG) was used to enable disulfide reshuffling in order to allow correct disulfide formations during refolding. Different GSH:GSSG ratios were experimentally tested and a 10-fold excess of GSH over GSSG found to be best to support correct disulfide bond formation. The His6-GB1 tag was cleaved by TEV protease and Yos9 MRH purified by reverse Ni–NTA chromatography followed by size exclusion chromatogrphay on a HiLoad 16/600 Superdex 75 pg column. The final molecular weight was 18.3 kDa.

NMR experiments and structure determination

NMR spectra were acquired on Bruker Avance spectrometers operating at proton frequencies of 600–950 MHz. All spectra were recorded at 303 K.

Spectra for backbone, side chain assignment and NOESY spectra were measured on uniformly ^{13}C,^{15}N-labeled Yos9 (90–249) or ^{15}N-labeled Yos9 (90–249) at concentrations ranging from 0.6 to 1.2 mM in buffer containing 25 mM HEPES (pH 7.0), 50 mM NaCl, 0.03% NaN3, protease inhibitor cocktail, DSS and 5% D_2O. Experiments on the carbohydrate bound Yos9 MRH were performed with a 15-fold molar excess of 3α, 6α mannopentaose (Sigma).

Backbone resonance assignments were obtained using BEST-TROSY versions of HNCACB, HN(CO)CACB, HN(CA)CO and HNCO experiments. Aliphatic side chain resonances were assigned using [^{15}N, ^{1}H]-TROSY-based versions of H(CCCO)NH-TOCSY (22.6 ms spin-lock time), (H)C(CCO)NH-TOCSY (22.6 ms spin-lock time) and HCCH-TOCSY (18.6 ms spin-lock time) experiments. Assignments for aromatic side chain resonances were obtained by a standard set of aromatic NMR experiments (Lohr et al. 2007; Yamazaki et al. 1993). Assignments were completed using 3D NOESY-HSQC experiments. All shifts were assigned manually with the help of the program NMRFAM-SPARKY.

Distance restraints resulted from a set of three 3D NOESY experiments (^{15}N-separated NOESY-TROSY at 950 MHz, ^{13}C-separated NOESY-HSQC of the aliphatic region at 800 MHz and ^{13}C-separated NOESY-ct-TROSY of the aromatic region at 700 MHz), all recorded with mixing times of 70 ms. Peak lists served as inputs for structure calculations using the program CYANA (Güntert and Buchner 2015; Güntert et al. 1997). In addition to distance restraints, dihedral angle restraints obtained by the TALOS + software (Shen et al. 2009) were used. The 20 best structures according to their target function value were energy-minimized with the program OPALp (Koradi et al. 2000) and selected for presentation. Structures and chemical shifts were deposited in the Protein Data Bank (PDB) and in the Biological Magnetic Resonance Bank (BMRB) under the accession codes 6F99 and 34218 (Yos9 MRH) and 6F9A and 34219 (Yos9 MRH complex with 3α, 6α mannopentaose), respectively. Structural statistics can be found in Tables 1 and 2.

$^{13}C/^{15}N$-filtered NOESY-[^{13}C, ^{1}H]-sfHMQC (aromatic region; 150 ms mixing time) and $^{13}C/^{15}N$-filtered NOESY-[^{13}C, ^{1}H]-HSQC (aliphatic region; 250 ms mixing time)

Table 1 Structural statistics of Yos9 MRH (90–249)

NOE assignment[a]	CYANA result	Energy-minimized[b]
^{15}N-resolved NOESY cross peaks	2160	
^{13}C-resolved NOESY cross peaks	5039	
^{13}C-resolved aromatic NOESY cross peaks	661	
Total number of NOESY cross peaks	7860 (100%)	
Assigned cross peaks[d]	6642 (84.5%)	
Unassigned cross peaks[d]	1218 (15.5%)	
Structural restraints		
Assigned NOE distance restraints[e]	3610 (100%)	
Short range $\|i-j\| \leq 1$	1705 (47.2%)	
Medium range $1 < \|i-j\| < 5$	537 (14.9%)	
Long range $\|i-j\| \geq 5$	1368 (37.9%)	
Dihedral angle restraints (φ/ψ)	250	
Structure statistics		
Average CYANA target function value (Å^2)	1.94 ± 0.09	3.60 ± 0.50
Average AMBER Energies (kcal/mol)	-5004.46 ± 144.38	-6419.61 ± 128.60
Restraint violations[c]		
Max. distance restraint violation (Å)	0.45	0.13
Number of violated distance restraints > 0.2 Å	0	0
Max. dihedral angle restraint violations (°)	8.29	6.67
Number of violated dihedral angle constraints > 5°	2	1
Ramachandran plot		
Residues in most favored regions	82.6%	85.6%
Residues in additionally allowed regions	17.2%	13.9%
Residues in generously allowed regions	0.2%	0.5%
Residues in disallowed regions	0.0%	0.0%
RMSD (residues 94..140, 156..209, 215..246)		
Average backbone RMSD to mean (Å)	0.27 ± 0.05	0.33 ± 0.05
Average heavy atom RMSD to mean (Å)	0.59 ± 0.06	0.65 ± 0.05

[a]Using automated NOE assignment and structure calculation functionalities of CYANA

[b]After restrained energy minimization with OPALp

[c]After energy minimization, calculated with CYANA

[d]In parenthesis the percentage of the total number of cross peaks

[e]In parenthesis the percentage of the total number of distance restraints from the peak assignment

were used to detect cross peaks between protein CH- groups and H atoms of the carbohydrate in order to define residues in contact with 3α, 6α mannopentaose.

Measuring binding affinity

The binding affinity of 3α, 6α-mannopentaose to Yos9 was determined by measuring tryptophan fluorescence. 1 µM Yos9 was diluted (1:25) into the reaction buffer (25 mM HEPES, pH 7.0, 50 mM NaCl) and 3α, 6α-mannopentaose was titrated to final concentrations ranging from 0 to 26 µM. Fluorescence spectra (320–450 nm) were measured with exciting the protein at 295 nm. After quantifying the maximum of the emission spectra at 340 nm and calculating the differences to the spectrum without 3α, 6α-mannopentaose, the resulting hyperbolic binding curve was fitted assuming a standard 1:1 binding mode resulting in a K_D value of 16.17 ± 2.52 µM.

Results

Yos9 consists of a signaling peptide responsible for targeting the protein to the ER lumen, a mannose 6-phoshate receptor homology (MRH) domain and a dimerization domain (DD), followed by a largely unstructured region. So far, structural studies of Yos9 are limited to its dimerization domain (Hanna et al. 2012). In order to allow structural and interaction studies of the MRH domain of Yos9, we determined the correct sequence boundaries by screening a variety of different ^{15}N-labeled Yos9 protein constructs by [^{15}N, ^{1}H]-HSQC experiments. Guided by a sequence alignment

Table 2 Structural statistics of Yos9 MRH (90–249) bound to 3α, 6α-mannopentaose

NOE assignment[a]	CYANA result	Energy-minimized[b]
^{15}N-resolved NOESY cross peaks	1986	
^{13}C-resolved NOESY cross peaks	5684	
^{13}C-resolved aromatic NOESY cross peaks	532	
Total number of NOESY cross peaks	8202 (100%)	
Assigned cross peaks[d]	6716 (81.9%)	
Unassigned cross peaks[d]	1486 (18.1%)	
Structural restraints		
Assigned NOE distance restraints[e]	3885 (100%)	
Short range $\|i-j\| \leq 1$	1773 (45.6%)	
Medium range $1 < \|i-j\| < 5$	563 (14.5%)	
Long range $\|i-j\| \geq 5$	1549 (39.9%)	
Dihedral angle restraints (φ/ψ)	248	
Structure statistics		
Average CYANA target function value (Å^2)	1.33 ± 0.10	3.46 ± 0.52
Average AMBER energies (kcal/mol)	-5045.07 ± 125.14	-6444.60 ± 110.82
Restraint violations[c]		
Max. distance restraint violation (Å)	0.38	0.12
Number of violated distance restraints > 0.2 Å	1	0
Max. dihedral angle restraint violations (°)	6.55	7.29
Number of violated dihedral angle constraints > 5°	2	1
Ramachandran plot		
Residues in most favored regions	77.7%	83.0%
Residues in additionally allowed regions	22.3%	16.7%
Residues in generously allowed regions	0.0%	0.2%
Residues in disallowed regions	0.0%	0.0%
RMSD (residues 94..140, 156..209, 215..246)		
Average backbone RMSD to mean (Å)	0.24 ± 0.03	0.30 ± 0.03
Average heavy atom RMSD to mean (Å)	0.57 ± 0.04	0.63 ± 0.04

[a]Using automated NOE assignment and structure calculation functionalities of CYANA

[b]After restrained energy minimization with OPALp

[c]After energy minimization, calculated with CYANA

[d]In parenthesis the percentage of the total number of cross peaks

[e]In parenthesis the percentage of the total number of distance restraints from the peak assignment

with the MRH domain of its human homologue OS-9, which was solved by X-ray crystallography (Satoh et al. 2010), a construct comprising residues 115–240 was considered as being sufficient. Secondary structure predictions, however, indicated an additional helical region directly preceding the MRH domain of Yos9 (92–114). We therefore, expressed a set of different N- and C-terminally elongated versions of the core MRH domain and investigated its structural integrity by NMR spectroscopy (Fig. 1). This investigation revealed a construct comprising residues 90–249 as the minimal MRH domain, with further N- or C-terminally shortened versions showing significant chemical shift perturbations indicating that these regions interact with the core β-sheet structure. The region between residues 249 and 262 is dispensable since the removal of these 13 amino acids induces no chemical shift perturbations in the MRH domain. A construct encompassing also the region that is N-terminal of the predicted MRH core domain (32–249) added only peaks with chemical shifts characteristic of unfolded sequences thereby suggesting that this region is largely unstructured and not interacting with the MRH core structure (Fig. 2).

Subsequently, the optimized Yos9 (90–249) construct was expressed in a ^{13}C,^{15}N-labeled form and all backbone and side chain resonances were assigned with a standard set of TROSY-based triple resonance experiments. Distance restraints were derived from ^{15}N-separated as well as ^{13}C-separated NOESY-HSQC spectra (one centered on the aromatic region and one on the aliphatic region). The solution structure of the free MRH domain was calculated using CYANA (Güntert and Buchner 2015; Güntert et al. 1997). The calculation was based on 3610 assigned NOE distance restraints including a total of 1368 long range ($|i-j| \geq 5$)

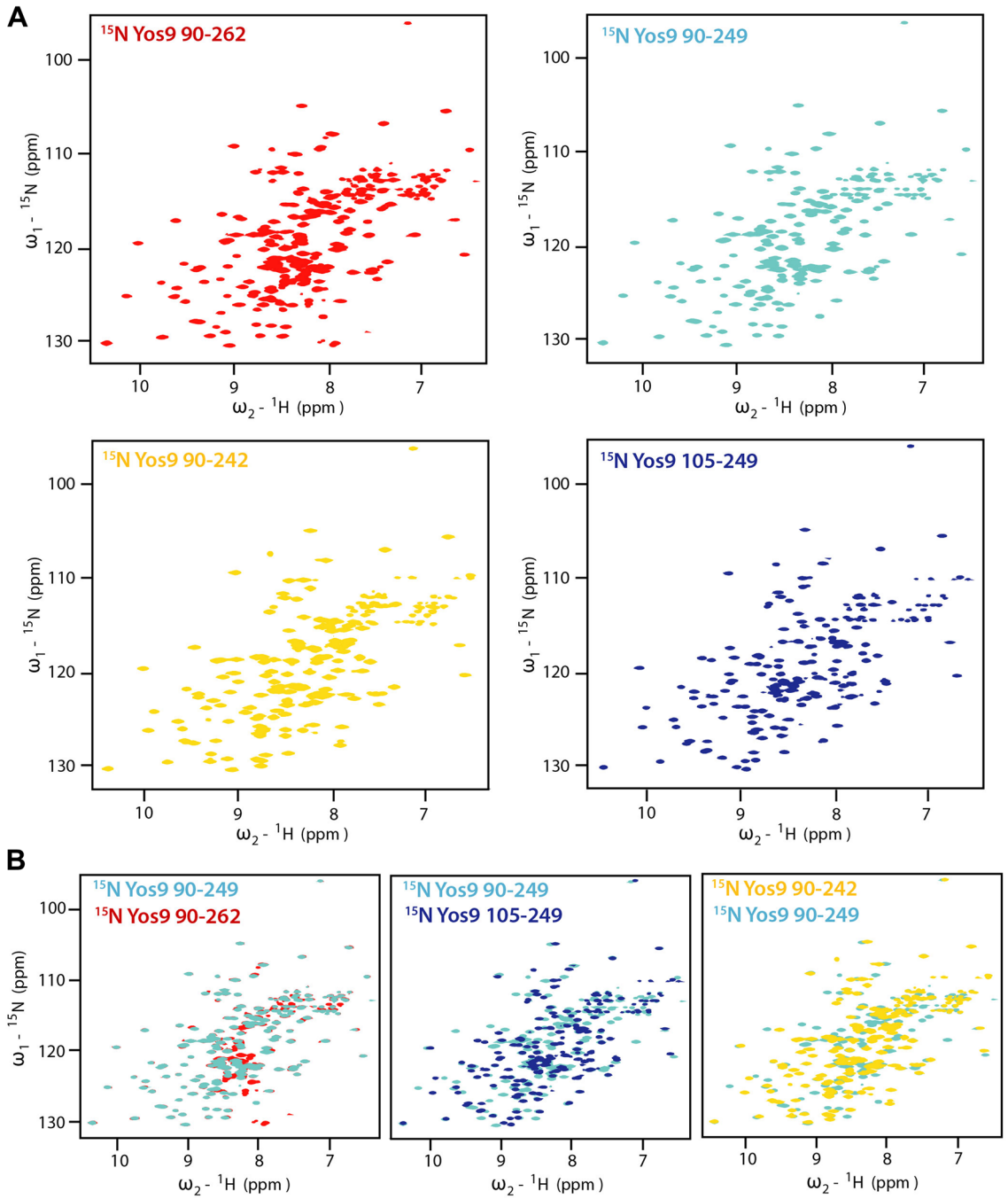

Fig. 1 Construct optimization of the Yos9 MRH domain for NMR. **a** [^{15}N,^{1}H]-TROSY HSQC spectra of ^{15}N-labeled Yos9 MRH domain constructs 90–262, 90–249, 90–242 and 105–249. The spectra show well dispersed signals except for the construct 90–262 which has significant overlap in the central region of the spectrum. Yos9 (90–249) was identified as the optimal NMR construct **b** Pairwise superposition of HSQC spectra of different Yos9 constructs with the spectrum of the optimal Yos9 (90–249) construct. Removal of residues 250–262 results in no detectable chemical shift perturbations (left), whereas removal of residues 90–104 or residues 243–249 induced significant chemical shift perturbations in the entire MRH domain. This shows that these regions are folded and associated with the MRH core structure

restraints and 250 dihedral angle restraints (φ/ψ) obtained with the TALOS + software (Shen et al. 2009) (Table 1).

The Yos9 MRH domain consists of a β-barrel structure similar to its human homologue OS-9. The most obvious difference between the OS-9 and the Yos9 structures is the long N-terminal helix of Yos9. This helix (residues 92–114) interacts with a short C-terminal helix, also present in the OS-9 structure, in an antiparallel manner. As a consequence

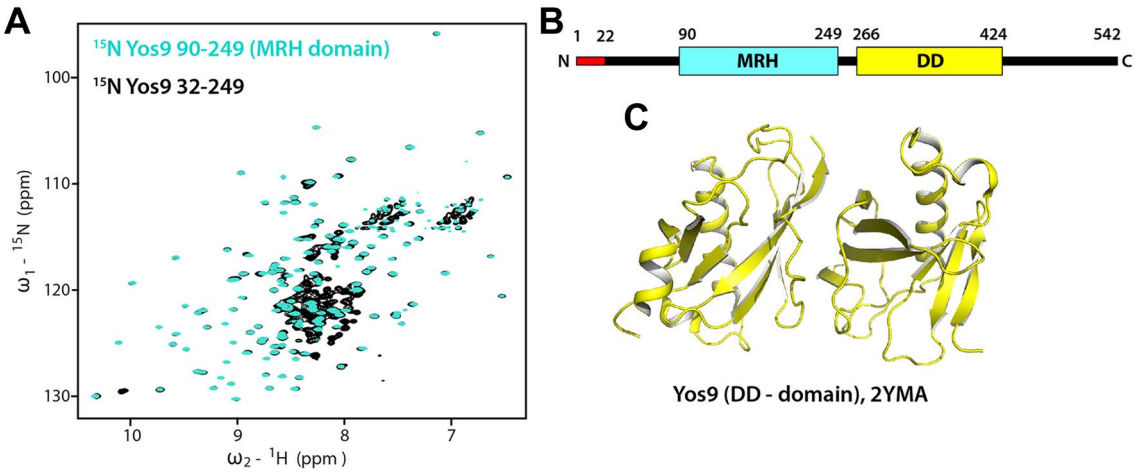

Fig. 2 HSQC spectrum of Yos9 (32–249) and domain organization of Yos9. **a** Overlay of HSQC spectra of Yos9 (32–249) and Yos9 (90–249). **b** Domain organization of full-length Yos9. The signal sequence for ER import is shown in red. This region is followed by an unstructured N-terminal region, the MRH domain, a short linker, the DD domain and a largely unstructured C-terminal domain. **c** Structure of the Yos9 dimerization domain (DD). PDB code: 2YMA (Hanna et al. 2012)

of this helical interaction, the β5–β6 strands adopt a very different position compared to the OS9 crystal structure. In particular the orientation of strand β5 in the OS-9 structure would clash with the N-terminal helix, requiring relocation. A further significant difference is the length of the β3β4 loop that is seven amino acids longer in the Yos-9 structure (Fig. 3c).

To investigate the interaction of the MRH domain with glycans, we added a glycan-mimicking carbohydrate (3α, 6α-mannopentaose), which exposes a terminal α1,6-linked mannose residue to a ^{15}N-labeled sample of the MRH domain. Significant chemical shift changes occurred for almost all backbone amide resonances prompting us to determine the structure of the MRH domain in its complexed form to investigate potential structural rearrangements. The structure of the bound conformation of the Yos9 MRH domain was based on 3885 NOE distance restraints (1549 long range restraints) and 248 dihedral angle restraints (Table 2). The two structure ensembles are superimposed in Fig. 3a, b and are well-defined except for the β3β4 loop region (residues 141–155). The backbone root-mean-square deviation of the mean structures of the complexed and uncomplexed forms is 1.2 Å including only the regular secondary structure elements. The overlay of both structures also reveals that binding of the carbohydrate induces a reorientation of several loops (Fig. 3b), most prominently the β1β2, β6β7 and β8β9 loops. Interestingly, the distance between the β1β2 and β6β7 loops is significantly decreased in the bound form, suggesting that these loops wrap around the bound carbohydrate. The β8β9 loop seems to additionally close the binding pocket. By contrast, OS-9 was only solved in complex with its sugar ligand, thereby revealing no information about these motions. These rearrangements might define an additional signal that is transmitted to nearby components in the HRD1 ligase complex. This signal might be required to hand over a misfolded client protein that was successfully scanned for the correct glycan structure to membrane components that are responsible for translocation.

The two NMR structures provide insights into the structural rearrangements that the protein experiences upon binding of the sugar. The two structures also explain why the addition of 3α, 6α-mannopentaose resulted in chemical shift perturbations of not only residues close to or at the glycan binding site, but significantly affected also backbone amides of the β1 and β3 strands or at the C-terminal end of the N-terminal helix (Fig. 4a, b). Since the movement of the loop regions of the carbohydrate binding pocket is rigidly connected to the β-barrel structure, the bending of β-strands 5–9 is also affected. This in turn further affects the relative orientation of the helix and the β-barrel, thereby explaining also chemical shift perturbations on the helix upon carbohydrate binding (Movie 1).

We measured filtered NOESY experiments to prove that the carbohydrate only binds to the site known from the OS-9 structure and to show that chemical shift perturbations far from the binding site are due to the conformational changes described above and not due to additional interaction sites. These experiments allowed us to unambiguously identify key residues on Yos9 that are in direct contact to the sugar. These residues form a contiguous surface and are shown in Fig. 4c. The surface resembles the site found by superimposing the OS-9 sugar complex and the Yos9 structure (Fig. 3c).

Previous analyses have shown that OS-9 recognizes the glycan structure using a double tryptophan motif (W117 and

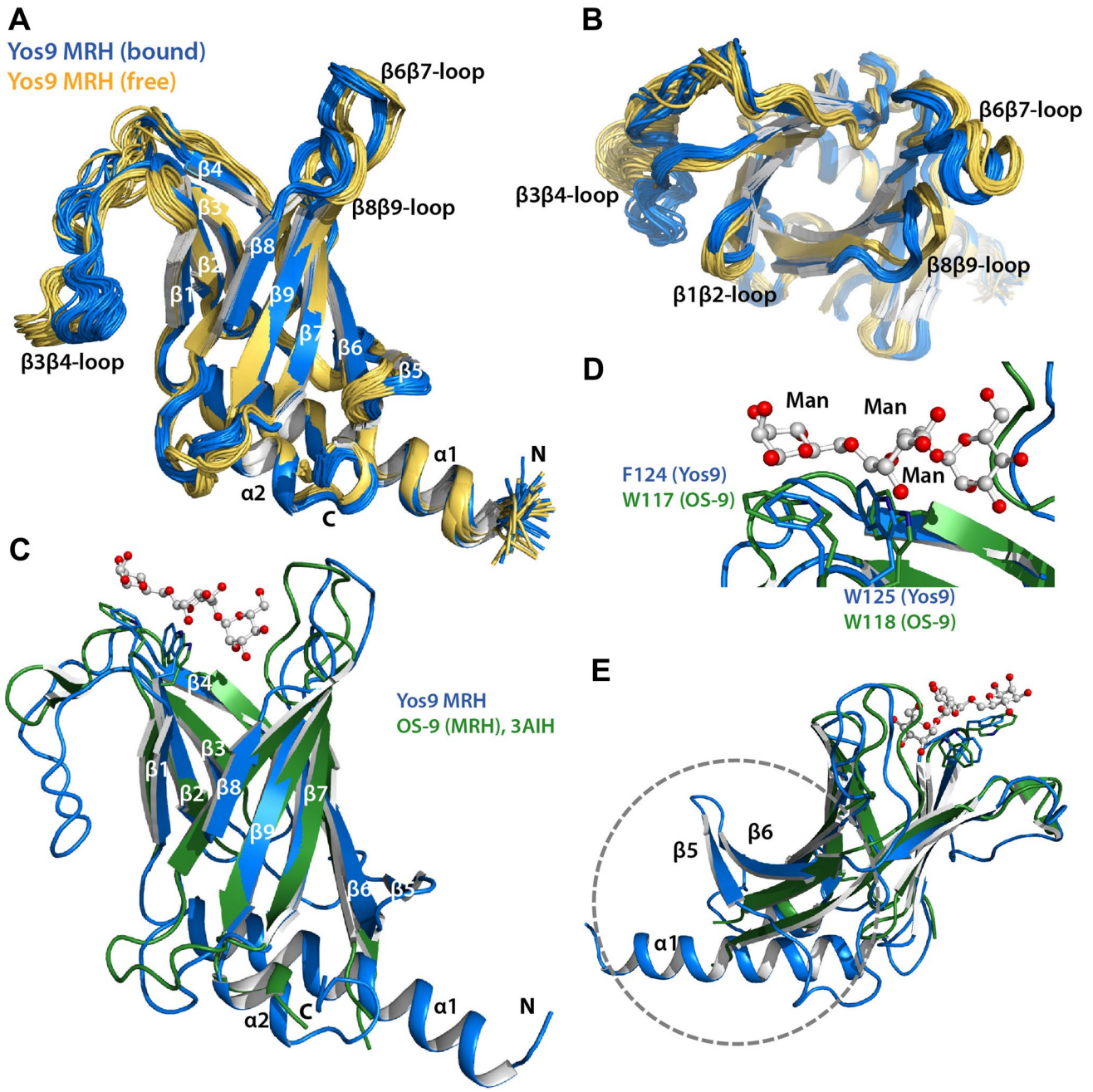

Fig. 3 Glycan binding results in a conformational change of Yos9 and comparison of Yos9 and OS-9 MRH domains. **a** Superposition of the NMR solution structure ensemble for Yos9 (20 structures) in its two conformational states, free (yellow) and bound to 3α, 6α-mannopentaose (blue). **b** Top view of the glycan recognition site at one opening of the β-barrel. β1β2, β6β7 and β8β9 loop regions are reoriented in the sugar bound form and well-defined in both conformational states. The distance between the β1β2 and β6β7 loops is significantly decreased in the bound form suggesting that these loops wrap around the sugar. The β8β9 loop is additionally closing the binding pocket. **c** Structural comparison of the X-ray structure of OS-9 MRH (PDB code: 3AIH) and the structure with the lowest target function of the structure ensemble of Yos9 MRH. Both proteins are shown in their ligand bound form. The sugar which was co-crystallized with the OS-9 MRH domain is also shown and binds to one opening of the β-barrel. Structural differences include, the additional helix α1, a longer β3β4 loop and the completely different arrangement of β-strand 5 and 6. **d** Comparison of the double WW motif of OS-9 and the FW motif involved in mannose binding. Side chain orientations of these aromatic residues are well conserved among both proteins. **e** Comparison of Yos9 and OS-9 as in C but in a different view to highlight the different arrangement of β-strand 5 and 6 in both β-barrel structures

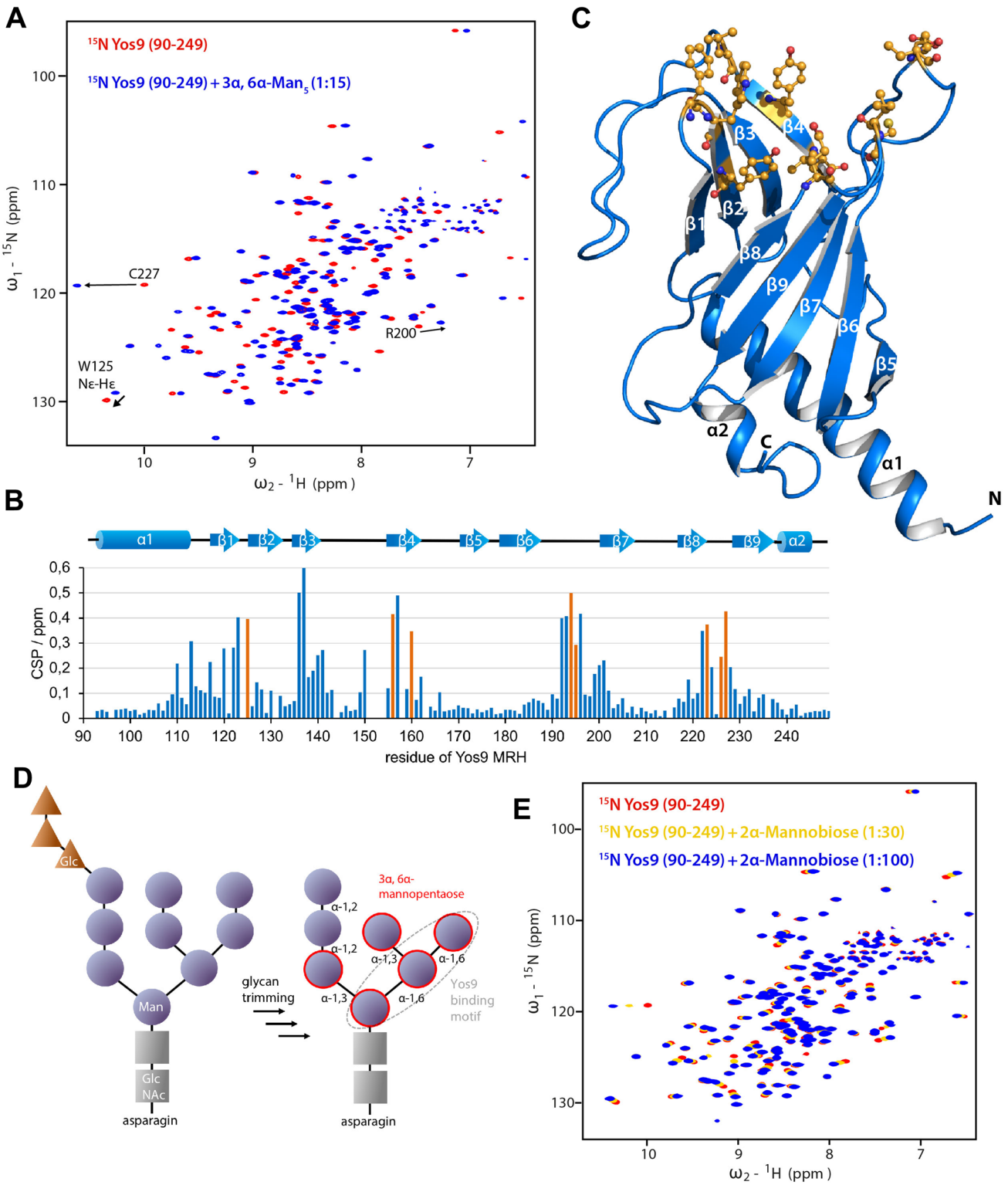

Fig. 4 NMR titration experiments showing carbohydrate binding activity and specificity of Yos9 MRH domain for terminally exposed α-1,6 mannose. **a** Overlay of [^{15}N,^{1}H]-HSQC spectra of Yos9 (90–249) in absence (red) and presence of 3α, 6α-mannopentaose (15-fold molar excess). Large regions of Yos9 are affected. **b** CSP analysis of Yos9 residues upon interaction with the sugar. Residue for which specific intermolecular NOEs have been detected are displayed in orange. This reveals that many shifts arise from conformational changes. **c** Mapping of residues on the Yos9 MRH structure that are in contact (NOEs were detected) with the sugar. **d** Schematic overview of the N-linked glycan trimming by ER glucosidases and mannosidases. The sugar used in NMR experiments is highlighted in red, the Yos9 binding motif is circled in grey. **e** NMR titration experiment of Yos9 and 2α-mannobiose

W118) (Satoh et al. 2010). In Yos9 this motif is replaced with a phenylalanine- tryptophane-motif (F124 and W125) that is stabilized by an CH–π interaction (Fig. 3d). Yos9 recognizes the C-branch of glycans that were processed by Htm1 to expose a terminal α1,6-linked mannose residue. Figure 4d summarizes the glycan processing in the ER and highlights the Yos9 recognition motif as well as the sugar that was experimentally used (Fig. 3d). To investigate whether Yos9 shows an intrinsic sugar binding propensity that does not require the correct linkage, we titrated the MRH domain with increasing amounts of 2α-mannobiose that contains a single α1,2-linkage between two mannose moieties (Fig. 4d). A weak interaction in the fast-exchange regime was observed (Fig. 4e). However, even at a 100-fold molar excess of the sugar saturation could not be achieved. In contrast, binding of the correct ligand, 3α, 6α-mannopentaose, is strong with a K_D of 16 µM (measured using tryptophan fluorescence). Interestingly, 2α-mannobiose was not able to induce the same chemical shift perturbations that we observed for 3α, 6α-mannopentaose. This suggests that the glycan binding site might be composed of a region that is pre-formed for binding to mannose independent from the type of glycosidic bond that connects the mannose residues, as well as a region that senses the terminal α1,6-linked mannose at the C-arm of the glycan via conformational change of the β6β7 and β8β9 loops. This might represent a scanning-like mechanism where the MRH domain is capable of binding mannose residues independent of their linkages. However, in case the correct signal is recognized, a conformational transition enables higher-affinity interactions.

Discussion

The MRH domain of Yos9 shares ~ 25% sequence similarity with its human homologue and is composed of a central β-barrel seen also in the OS-9 structure (Satoh et al. 2010). Unlike OS-9, however, the Yos-9 β-barrel is closed on one side by a unique ~ 20 amino acids long α helix. Such a helical element has not been observed so far within MRH domains. The existence of this additional structural element significantly restricts the arrangement of the nine β-strands of the MRH domain and results in a different arrangement of strands β5 and β6 that would otherwise collide with the helix.

Comparison of the NMR structures in the free and in the oligosaccharide-bound form reveals insights into glycan recognition by Yos9. We detected significant backbone reorientations that were not restricted to the binding region of the ligand. In particular the distances between loops β1β2, β6β7 and β8β9 decrease upon ligand binding. This suggest a gripping movement of those regions. The MRH domain of the β subunit of glucosidase II has also been solved in a free and bound form (complexed with mannose). But unlike Yos9 only repositioning of side chains were observed without any major differences in the protein backbone (Olson et al. 2013). The fact that only Yos9 exhibits those large rearrangements might suggest that this constitutes an additional signal that is required to hand over misfolded client proteins to nearby components of the HRD1 ligase complex. Yos9 has the difficult task to select only the correctly processed glycan structures on the C-arm that expose a terminal α1,6-linked mannose. By contrast, glucosidase II performs initial trimming of glucose on the A-branch of the N-linked glycans (Stigliano et al. 2009) and its MRH domain recognizes mannose residues either localized on the B and/or C-arm of the glycan (Hu et al. 2009; Stigliano et al. 2011). Therefore, it can be speculated that the existence of conformational transitions in MRH domains can be either due to specificity requirements and/or might define an additional signal for other downstream components.

Glycan-binding of Yos9 involves a FW motif that superimposes well with the WW-motif on OS-9 in a structural alignment. This indicates that the sugar binding pocket for recognizing the trimmed C-arm is well conserved. Since also binding of Yos9 to α1,2-linked mannose was observed by NMR, the glycan site might be composed of a region that has an inherent affinity for mannose and a region that senses the terminal α1,6-linked mannose via conformational motion of the β6β7 and β8β9 loops. This would represent a scanning like mechanism that ensures that only correctly processed glycans induce the conformational changes in the Yos9 MRH domain. A previous study has suggested that the Hrd3 binding site lies within the herein structurally determined MRH domain of Yos9 (Hanna et al. 2012). Therefore, further studies have to focus on the Hrd3-Yos9 interaction.

Acknowledgements This work was funded by the Deutsche Forschungsgemeinschaft (SFB 740, SFB 1177) and the Center for Biomolecular Magnetic Resonance (BMRZ) at the Goethe University Frankfurt.

References

Aebi M (2013) N-linked protein glycosylation in the ER. Biochim Biophys Acta 1833:2430–2437

Braakman I, Bulleid NJ (2011) Protein folding and modification in the mammalian endoplasmic reticulum. Annu Rev Biochem 80:71–99

Clerc S, Hirsch C, Oggier DM, Deprez P, Jakob C, Sommer T, Aebi M (2009) Htm1 protein generates the N-glycan signal for glycoprotein degradation in the endoplasmic reticulum. J Cell Biol 184:159–172

D'Alessio C, Dahms NM (2015) Glucosidase II and MRH-domain containing proteins in the secretory pathway. Curr Protein Pept Sci 16:31–48

Gauss R, Kanehara K, Carvalho P, Ng DT, Aebi M (2011) A complex of Pdi1p and the mannosidase Htm1p initiates clearance of unfolded glycoproteins from the endoplasmic reticulum. Mol Cell 42:782–793

Güntert P, Buchner L (2015) Combined automated NOE assignment and structure calculation with CYANA. J Biomol NMR 62:453–471

Güntert P, Mumenthaler C, Wüthrich K (1997) Torsion angle dynamics for NMR structure calculation with the new program DYANA. J Mol Biol 273:283–298

Hanna J, Schutz A, Zimmermann F, Behlke J, Sommer T, Heinemann U (2012) Structural and biochemical basis of Yos9 protein dimerization and possible contribution to self-association of 3-hydroxy-3-methylglutaryl-coenzyme A reductase degradation ubiquitin-ligase complex. J Biol Chem 287:8633–8640

Hosokawa N, Kamiya Y, Kamiya D, Kato K, Nagata K (2009) Human OS-9, a lectin required for glycoprotein endoplasmic reticulum-associated degradation, recognizes mannose-trimmed N-glycans. J Biol Chem 284:17061–17068

Hu D, Kamiya Y, Totani K, Kamiya D, Kawasaki N, Yamaguchi D, Matsuo I, Matsumoto N, Ito Y, Kato K et al (2009) Sugar-binding activity of the MRH domain in the ER alpha-glucosidase II beta subunit is important for efficient glucose trimming. Glycobiology 19:1127–1135

Jakob CA, Bodmer D, Spirig U, Battig P, Marcil A, Dignard D, Bergeron JJ, Thomas DY, Aebi M (2001) Htm1p, a mannosidase-like protein, is involved in glycoprotein degradation in yeast. EMBO Rep 2:423–430

Koradi R, Billeter M, Güntert P (2000) Point-centered domain decomposition for parallel molecular dynamics simulation. Comput Phys Commun 124:139–147

Lohr F, Hansel R, Rogov VV, Dotsch V (2007) Improved pulse sequences for sequence specific assignment of aromatic proton resonances in proteins. J Biomol NMR 37:205–224

Olson LJ, Orsi R, Alculumbre SG, Peterson FC, Stigliano ID, Parodi AJ, D'Alessio C, Dahms NM (2013) Structure of the lectin mannose 6-phosphate receptor homology (MRH) domain of glucosidase II, an enzyme that regulates glycoprotein folding quality control in the endoplasmic reticulum. J Biol Chem 288:16460–16475

Pfeiffer A, Stephanowitz H, Krause E, Volkwein C, Hirsch C, Jarosch E, Sommer T (2016) A complex of Htm1 and the oxidoreductase Pdi1 accelerates degradation of misfolded glycoproteins. J Biol Chem 291:12195–12207

Quan EM, Kamiya Y, Kamiya D, Denic V, Weibezahn J, Kato K, Weissman JS (2008) Defining the glycan destruction signal for endoplasmic reticulum-associated degradation. Mol Cell 32:870–877

Satoh T, Chen Y, Hu D, Hanashima S, Yamamoto K, Yamaguchi Y (2010) Structural basis for oligosaccharide recognition of misfolded glycoproteins by OS-9 in ER-associated degradation. Mol Cell 40:905–916

Shen Y, Delaglio F, Cornilescu G, Bax A (2009) TALOS+: a hybrid method for predicting protein backbone torsion angles from NMR chemical shifts. J Biomol NMR 44:213–223

Stigliano ID, Caramelo JJ, Labriola CA, Parodi AJ, D'Alessio C (2009) Glucosidase II beta subunit modulates N-glycan trimming in fission yeasts and mammals. Mol Biol Cell 20:3974–3984

Stigliano ID, Alculumbre SG, Labriola CA, Parodi AJ, D'Alessio C (2011) Glucosidase II and N-glycan mannose content regulate the half-lives of monoglucosylated species in vivo. Mol Biol Cell 22:1810–1823

Szathmary R, Bielmann R, Nita-Lazar M, Burda P, Jakob CA (2005) Yos9 protein is essential for degradation of misfolded glycoproteins and may function as lectin in ERAD. Mol Cell 19:765–775

von Delbruck M, Kniss A, Rogov VV, Pluska L, Bagola K, Lohr F, Güntert P, Sommer T, Dötsch V (2016) The CUE Domain of Cue1 Aligns Growing Ubiquitin Chains with Ubc7 for Rapid Elongation. Mol Cell 62:918–928

Werner ED, Brodsky JL, McCracken AA (1996) Proteasome-dependent endoplasmic reticulum-associated protein degradation: an unconventional route to a familiar fate. Proc Natl Acad Sci USA 93:13797–13801

Yamazaki T, Forman-Kay JD, Kay LE (1993) Two-dimensional NMR experiments for correlating carbon-13.beta. and proton. delta./.epsilon. chemical shifts of aromatic residues in 13C-labeled proteins via scalar couplings. J Am Chem Soc 115:11054–11055